The last decade has seen a proliferation of studies of active dendrites, propelled by a number of simultaneous technical advances: (1) patch-clamp recordings in brain slices that allow for very high-quality records of somatic and dendritic electrical signals (Edwards et al., 1989; Stuart and Spruston, 1995), (2) calcium-dependent fluorescent dyes that enable the dynamics of intracellular free calcium in dendrites and even spines (e.g., Fig. 12.14) to be accurately recorded (Tsien, 1988, 1989), and (3) new forms of visible and infrared microscopy for high-resolution imaging of dendrites in brain slices as well as in the living animal (Fine et al., 1988; Denk, Strickler, and Webb, 1990; Dodt and Zieglgänsberger, 1994).

We cannot do justice to this gargantuan literature. Instead, we follow the excellent survey article by Mainen and Sejnowski (1998) and provide this brief synopsis. We will expand upon this, as necessary, further below.

1. Ionic channels from all major families of sodium, calcium, and potassium channels have been identified in dendrites. This includes both a very rapid and a sustained sodium current, low- and high-voltage activated calcium currents as well as sustained and transient potassium currents (Johnston et al., 1996; Hoffman et al., 1997).

2. Some types of channels are confined to specific compartments, such as the soma, initial segment, dendritic shaft, or even spines (Westenbroek, Merrick, and Catterall, 1989; Westenbroek, Ahlijanian, and Catterall, 1990; Westenbroek et al., 1992; Turner et al., 1994; Denk, Sugimori, and Llinás, 1995).

3. Voltage-gated channel densities estimated by patch-clamp recording in dendrites generally are less than 10 channels per square micrometer of membrane. This should be contrasted with the 1000–2000 fast sodium channels per square micrometer found at the axonal node of Ranvier (Ritchie, 1995). A possible exception appear to be A-like transient potassium channels in the distal dendritic tree of pyramidal cells (Hoffman et al., 1997).

19.1.1 Fast Dendritic Spikes

The earliest evidence for rapid all-or-none events in the dendrites comes from hippocampal pyramidal and cerebellar Purkinje cells (Spencer and Kandel, 1961; Llinás et al., 1968; Llinás and Nicholson, 1971). The later observations were particularly convincing and conjured up a view of the Purkinje cell where the somatic membrane produces conventional fast sodium spikes, while the extended dendritic tree can generate fast sodium spikes, slower calcium spikes (see Fig. 6.1G), as well as so-called *plateau potentials*, long-lasting and graded depolarizations (Llinaás and Sugimori, 1980, 1992; Regehr, Konnerth, and Armstrong, 1992).

Of great interest has been the question of whether conventional action potentials, triggered at or near the cell body, propagate not only forward along the axon but also backward, into the dendritic tree. It was Ramón y Cajal (1909, 1991) who postulated the law of *dynamic polarization*, which stipulates that dendrites and cell bodies are the receptive areas for the synaptic input, and that the resulting output pulses are transmitted unidirectionally along the axon to its targets.

The classical description of spiking in a neuron derives from motoneurons (Coombs, Curtis, and Eccles, 1957; Fatt, 1957; Fuortes, Frank, and Becker, 1957). Here, action potential initiation normally occurs in a proximal segment of the axon, in a specialized region between the soma and the axon proper, called *axon hillock* or *initial segment*, that is

also the target of a particular type of inhibitory synapse (Farinas and DeFelipe, 1991). Yet when the motoneuron is strongly stimulated, spikes can be initiated in the dendrites.

Both *orthodromic*, that is, from the dendrites into the soma and axon, and *antidromic spike propagation*, from the cell body back into the dendrite has been inferred in pyramidal cells (e.g., Turner et al., 1991). Unambiguous observation of antidromic spike invasion had to await dual somatic-dendritic recordings in neocortical and hippocampal pyramidal cells from mammalian brain slices (Stuart and Häusser, 1994; Stuart and Sakmann, 1994; Spruston et al., 1995; reviewed in Stuart et al., 1997; Fig. 19.1 and discussed further below).

These findings clearly violate Ramón y Cajal's law of dynamic polarization. Spike initiation in the dendrite has been observed in several *in vitro* preparations under frequently unphysiological conditions (e.g., clamping V_{soma} to between -90 and -100 mV, blocking all inhibition, and so on; Regehr et al., 1993; Turner, Meyers, and Barker, 1993). Whether or not anti- or orthodromic dendritic spikes can be observed under more natural conditions, in particular in response to sensory or motor stimuli in an intact animal remains an open issue (Svoboda et al., 1997).

19.2 Action Potential Initiation in Cable Structures

A full grasp of the interplay between synaptic and voltage-gated currents on the one hand and the neuronal geometry on the other requires a detailed understanding of the nature of spike initiation. What determines the conditions under which an action potential can be triggered in excitable cable structures? The intuitive answer is to look to the properties

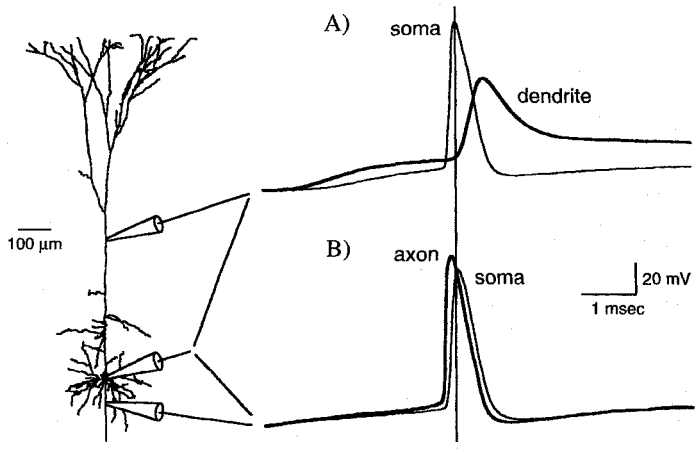

Fig. 19.1 Action Potential Initiation in a Pyramidal Cell Drawing of a layer 5 neocortical pyramidal cell from a 4-week-old rat slice preparation. The approximative locations of the sites of the dendritic, somatic, and axonal recordings are indicated. **(A)**, **(B)** Simultaneous patch-pipette recordings of action potentials elicited by threshold synaptic stimulations (Stuart et al., 1997). Dendritic and axonal recordings (heavy lines) are 270 μm and 17 μm, respectively, from the soma and are from different cells. V_{th} at the soma is 13 mV **(A)** and 15 mV **(B)** relative to the resting potential. The vertical line corresponds to the occurrence of the peak of the somatic membrane potential. Here, the action potential is always triggered in the axon, subsequently propagating back through the soma into the dendritic tree. This is termed *antidromic spike invasion*. Reprinted by permission from Stuart et al., (1997).

(density, kinetics, and type) of the excitable channels at the site of spike initiation. In this view, the membrane voltage needs to exceed a critical value V_{th} at which point the net ionic current becomes inward (Sec. 17.3.3). This inward current will further depolarize the membrane, thereby starting the regenerative process that underlies the initiation of the action potential, as covered in considerable detail in Chap. 6 (recall, in particular, Fig. 6.6).

However, these considerations hold only for isopotential structures where the ionic current can only flow across the membrane. What effect do cable properties have upon V_{th} (Rushton, 1937; Noble and Stein, 1966; Jack, Noble, and Tsien, 1975; Regehr and Armstrong, 1994)? In the following, we will first dwell on the theoretical issue of how V_{th} for rapid Hodgkin–Huxley-like spikes depends on the local cable geometry before we treat detailed biophysical modeling studies that reproduce antidromic spike invasion.

19.2.1 Effect of Dendritic Geometry on Spike Initiation

A significant portion of the excitable current in a cable that is generated at the site of current injection flows longitudinally away from this site, rather than depolarizing the local membrane. To compensate for this current loss, the voltage threshold in the cable must exceed $V_{th}^{uniform}$, the voltage threshold in the corresponding isopotential structure. (For an early discussion of this, see Hodgkin and Rushton, 1946; Noble and Stein, 1966.) Indeed, the geometry of the neuron strongly affects the condition for spike initiation and, as we shall show below, there are cases where excitation can never be realized in cable structures while spikes could be obtained in the corresponding uniform case (see also Chap. 9 in Jack, Noble, and Tsien, 1975).

Figure 19.2A illustrates that V_{th} does, indeed, strongly depend on cable properties, as well as on the site of input application. Using the standard Hodgkin–Huxley equations at 20° C, $V_{th}^{uniform}$ is approximately 8 mV. In the other extreme of an infinitely long cylinder, the voltage threshold $V_{th}^{infinite}$ is about 17.5 mV (independent of the diameter d), more than twice that of the isopotential case. For cylinders of finite length L, V_{th} lies between these two extremes. As expected, V_{th} is closer to the uniform isopotential case when L is small and it approaches $V_{th}^{infinite}$ in cylinders with large L values.

In any finite cable structure, V_{th} will always depend on the site of polarization X, and sometimes quite strongly. For short cylinders (e.g., $L = 0.5$ or 1), the lowest V_{th}, closest to $V_{th}^{uniform}$, is at the center of the cylinder. In other words, in these cylinders the midpoint is, effectively, the most isopotential site. For exactly the same reason, the local delay D_{ii} at the center of these cylinders is the largest (Agmon-Snir and Segev, 1993; see also Sec. 2.4). When one moves toward the ends of the cylinder, V_{th} increases monotonically to reach a maximum at the sealed-end boundaries. The situation changes for electrically longer cylinders (e.g., $L = 2$ or 4) where the lowest V_{th} is near (but not at) the terminals rather than at the center, as was the case for shorter cylinders. The effect of the sealed-end terminals causes current to be discharged more slowly near the boundaries compared to other sites, lowering V_{th}. The same result holds also for the site where the local delay is maximal; in long cylinders D_{ii} is maximal near both ends rather than at the center of the cylinder (Agmon-Snir and Segev, 1993).

Observing V_{th} at the midpoint of a cable with $L = 4$ (or at the ends of the cable with $L = 2$), one notices that the voltage threshold is essentially equal to $V_{th}^{infinite}$. This implies that for spike initiation in a Hodgkin–Huxley cable, being two space constants away from the sealed-end boundary approximates an infinitely long cylinder. One may conclude that, for neurons with cable lengths of approximately $L = 1$, V_{th} is the lowest at (or very near) the

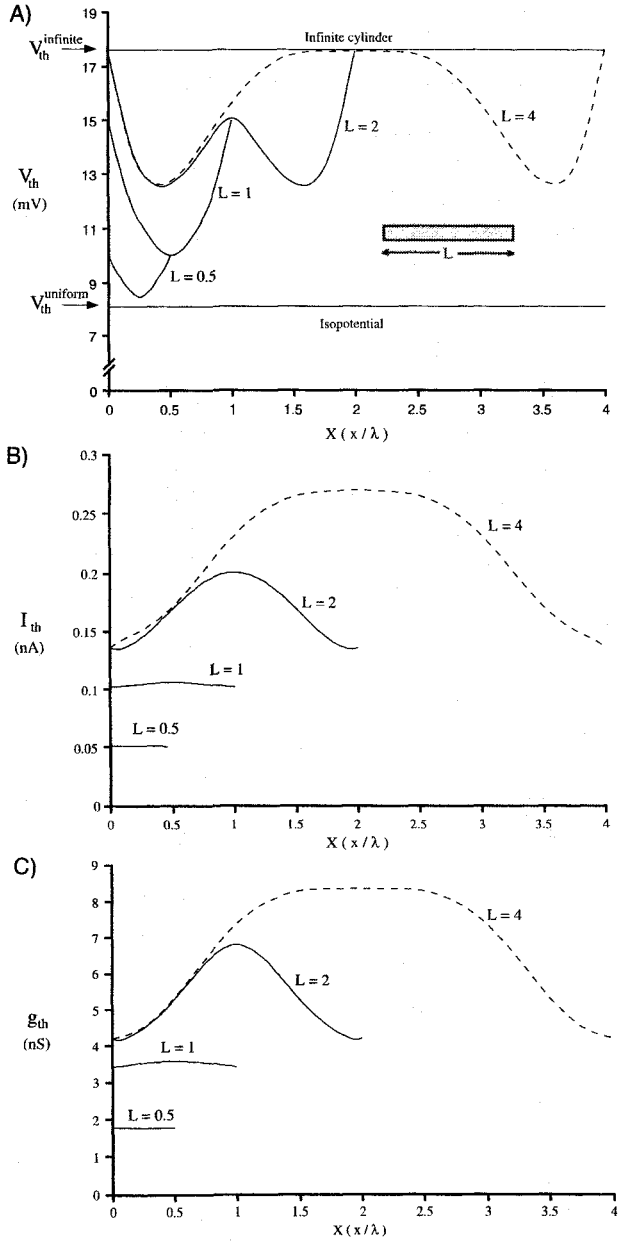

Fig. 19.2 Spike Initiation in a Single Cylinder **(A)** Voltage, **(B)** current, and **(C)** conductance thresholds for spike initiation in four different uniform cables of electrotonic length L endowed with Hodgkin–Huxley-like membrane as a function of the normalized location X of the input. **(A)** The input is a current stimulus of 0.5-msec duration (one-third of the passive membrane time constant) that was applied to different sites along the cable. The minimal voltage above rest at which a spike is initiated is defined to be V_{th}. The voltage threshold in any one cable can vary by up to 33% with X. **(B)** I_{th} is defined as the minimal amplitude of a sustained current able to initiate a spike. The dependency of the current threshold on the location of the stimulus is quite distinct from the dependency of V_{th} on X. For cables around $L = 1$, I_{th} only depends weakly on X. **(C)** The peak conductance of a single fast excitatory synaptic input was varied at different locations until a spike was initiated. This corresponds to a more physiological condition than the two previous panels. Qualitatively, g_{th} behaves as $I_{th}(t_{peak} = 0.3$ msec; $E_e = 0$ mV). All parameters of the Hodgkin–Huxley equations are as in Chap. 6, except that the temperature was set to 20° C. The cylinders have sealed end boundaries and a 2 μm diameter. Reprinted by permission from Rapp (1997).

midpoint of the structure. For neurons with a radial geometry, such as alpha motoneurons, cortical pyramidal neurons, spiny stellate cells, and so on (where the soma is situated near the "center of gravity" of the neuron), the geometry *per se* implies that the voltage threshold is lowest near the soma.

We argued in Sec. 17.3.4 that for slowly varying inputs, spike initiation occurs whenever a minimal current amplitude I_{th} (rather than a voltage threshold) is exceeded. How does this quantity vary with the length of the cylinder and the location of current injection? Based on Ohm's law and the fact that the input impedance in a finite cylinder is always lowest at

the center, $I_{th}(X)$ is expected to behave differently from $V_{th}(X)$. Figure 19.2B shows that this is indeed the case. Unlike V_{th}, which is always maximal at the ends of the cylinder, I_{th} is always minimal at these sites and peaks in the middle of the cable. And unlike V_{th}, which does not depend on the diameter of the fiber, but only on X, L, and the nature of the membrane itself, I_{th} is proportional to the total membrane area and thus scales with the diameter of the fiber. We conclude that in a finite-length segment of squid axon, the site for minimal threshold current for spike initiation is at the terminals.

As an aside, note that certain symmetry conditions are evident in Fig. 19.2. While V_{th} at the midpoint of cable of length L is always equal to V_{th} at the ends of the cable of length $L/2$, I_{th} at the center of the cable of length L is exactly twice that at the end of the cable of length $L/2$. This is the direct result of the symmetry of current flow when injected to the center of the cable (see also Rall, 1977).

Finally, Fig. 19.2C covers the more physiological situation of determining the minimal amplitude of a fast excitatory synaptic input sufficient to trigger a spike. The dependency of g_{th} on X and L parallels that of the current threshold.

Figure 19.3 treats spike initiation in a weakly excitable branched cable, corresponding to the situation prevalent in the apical dendrites of *in vitro* pyramidal cells (Stuart and Sakmann, 1994; Regehr and Armstrong, 1994; Magee and Johnston, 1995a,b; Spruston et al., 1995; Mainen et al., 1995; Rapp, Yarom, and Segev, 1996; Stuart et al., 1997). In particular, a low but uniform density of rapidly inactivating voltage-dependent Na^+ channels was reported along the apical dendrite up to at least 200 μm away from the cell body, channels that were no different from those found at the soma. The density is equivalent to about 4 mS/cm^2, or 1/30 its value in the squid giant axon (hence the attribute *weakly excitable*).

To illustrate the general principle involved, we chose an excitable cable whose total length is $L = 1$ and which branches at its midpoint (at $X = 0.5$) into two cylinders of unequal diameter (Fig. 19.3) such that Rall's (1959) $d^{3/2}$ rule holds.[1] Since the boundary condition is identical for both dendrites (sealed end) and their electrotonic length is also the same (0.5), the entire three-part cable can be reduced to a single equivalent cylinder (Sec. 3.2). This explains why V_{th} as a function of X should be symmetrical around the midpoint of the cable (lower curve in Fig. 19.3). Qualitatively, this curve looks similar to those seen in Fig. 19.2A except that, because of the much lower channel density, V_{th} is much higher than for a Hodgkin–Huxley cable and the points of lowest voltage threshold are at $X = 0.3$ and 0.7 (when delivering input simultaneously to both daughter branches).

Things change from the case of a strongly excitable cable when input is only delivered to a single daughter, say, the thick one (of 1.7 μm diameter). Now V_{th} diverges to infinity near the terminal of the cable. No input to the distal portion of the thick daughter branch can trigger an action potential (see the striped portion of the schematic in Fig. 19.3) because most of the—already small—excitable current generated locally flows within the cable and not across the membrane encasing the cable, and the regenerative process of the spike fails to start. This failure is much more dramatic in the thin ($d = 0.72$ μm) daughter branch where action potentials can only be triggered near the branch point. The large impedance load imposed by the rest of the dendritic tree onto thin branches implies that such arbors are unfavorable sites for spike initiation. In contrast, thicker (more proximal) branches in the same tree are more likely to be excited above threshold by local *polarization*.

1. One complication that we will not treat here is that the exact definition of what is meant by an action potential is rather involved for weakly excitable cables, given the smooth and continuous transition between a subthreshold and a suprathreshold response (see Rapp, 1997).

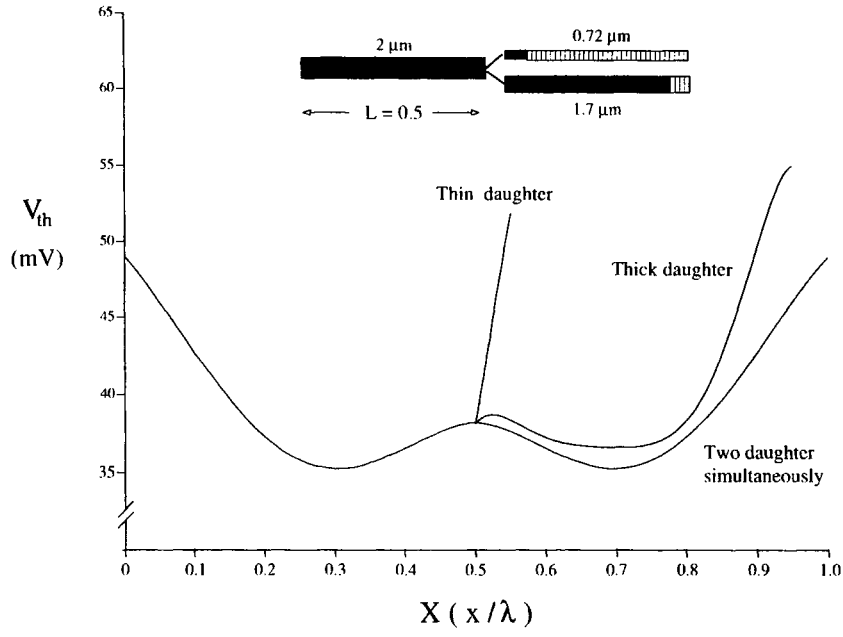

Fig. 19.3 SPIKE INITIATION IN A WEAKLY EXCITABLE BRANCHED DENDRITE Threshold conditions for spike initiation in a weakly excitable branched cable, mimicking the conditions believed to occur in the apical dendrite of neocortical pyramidal cells (Rapp, Yarom, and Segev, 1996). The parent dendrite splits into two 0.5λ-long cylinders of different diameters (see inset). The entire membrane is covered with sodium (and potassium) channels whose density is 1/15 of those of the standard Hodgkin–Huxley squid axon density. The voltage threshold (relative to V_{rest}) required to initiate a spike, is plotted as a function of the relative location of the stimulating electrode. The stimulus is a 15.3-msec-long current pulse delivered into the parent dendrite (left portion of the curve), into one or the other daughter branches, or into both branches simultaneously (right portion of both curves). No spikes can be initiated in the dashed portion of the two daughter branches in the inset. The membrane time constant is 46 msec. $\overline{G}_{Na} = 8$ mS/cm^2, $\overline{G}_K = 2.4$ mS/cm^2. The kinetics of the conductances were adapted to mimick neocortical pyramidal cells. Reprinted by permission from Rapp (1997).

As pointed out above, this situation changes when the stimulus is delivered simultaneously to both daughter branches. The lower right limb in Fig. 19.3 represents the case where the input current is applied simultaneously to the two daughter branches at sites with equal X values. The total current I_{stim} injected into each cable is split in proportion to their relative input conductances, that is, the current injected into the branch of diameter d_1 is equal to $I_{stim} d_1^{3/2}/(d_1^{3/2} + d_2^{3/2})$.

The result is striking (although directly expected from cable theory) in that a spike is now initiated in both branches, even at the distal sites of the thin branch. The reason for this improved efficiency of spike initiation is that the cable structure becomes effectively more isopotential, that is, less current flows longitudinally and more via the membrane. As we saw in Fig. 19.2, the excitation threshold is reduced for isopotential conditions. Finally, when receiving a distributed input as in Fig. 19.3, the threshold conditions in the branched cable are identical to those of the associated equivalent cylinder.

19.2.2 Biophysical Modeling of Antidromic Spike Invasion

To better understand these principles and to develop our intuition concerning anti- and orthodromic spike propagation, let us spend some time with Rapp, Yarom, and Segev (1996; see also Mainen et al., 1995, who come to much the same conclusions).

This study aims to reproduce the electrical events occurring in large layer 5 pyramidal cells recovered from the young rat cortex on the basis of a compartmental model. The apical tree extends by about 1 mm from the soma. Importantly, a large fraction of the associated axon is incorporated into the model: near the soma the axon's diameter is 2.8 μm, thinning to 0.5 μm in its fine collaterals.

What active currents need to be incorporated into this model? Pharmacological blockage of all calcium currents shows that they affect fast action potential propagation only minimally (Markram, Helm, and Sakmann, 1995), as does the sustained sodium current. The principal actor is a very rapid sodium current that peaks and inactivates within 1 msec following a voltage step (Stuart and Sakmann, 1994). Its kinetics, as well as that of a delayed rectifying potassium current, is modeled by an appropriately modified Hodgkin–Huxley scheme.

In a first step, Rapp, Yarom, and Segev (1996) homogeneously spread the Na^+ current throughout the dendrites, soma, and axon. At the low densities reported from the dendrites (3–4 channels per square micrometer, corresponding to 4.5–6 mS/cm^2; see Table 8.1) no full-blown action potentials can be generated at either dendritic or somatic sites. Increasing this density to an effective value of 12 mS/cm^2 enables a strong somatic input to generate a spike. This spike propagates back into the dendrites without any decrement, contrary to the experimental observation. Furthermore, dendritic stimulation leads to a local regenerative response that strongly attenuates on its way to the soma, failing to trigger a somatic spike.

This asymmetric behavior can be explained by recalling the asymmetry inherent in the voltage attenuation in a dendritic tree (Sec. 3.5.2 and Fig. 3.7): the voltage attenuates much more strongly when moving from a high- to a low-impedance site (that is, from the dendritic tree to the soma) than the other way around.

From the early motoneuron work cited above, it was known that action potentials can be trigged at lower voltages in the axon than in the soma. Dual intracellular recordings in hippocampal cells suggest that the normal site of initiation of fast action potentials is neither the soma nor the initial segment but the axon itself, possibly at the first node of Ranvier well away from the cell body (Colbert and Johnston, 1996). Indeed, the number of sodium channels measured in this study at the initial segment and soma is similar to that reported in the apical dendrites, around 3 to 4 per square micrometer. This not only suggests that the densities of sodium channels are substantially higher in the axon than at the soma (up to 2000 channels per square micrometer have been reported at the nodes of myelinated fibers; see Sec. 6.6) but also that their activation curve is shifted to more negative membrane potentials. Accordingly, Rapp, Yarom, and Segev (1996) use a low value for the sodium channels in the dendrites and a high value for the axon as well as shifting the sodium activation curve for the axonal sodium channels m_∞ by 10 mV to the left (see legend to Fig. 19.4). An alternative to the latter is to employ the same activation curves for dendrite and axon but a much, much higher axonal density (Mainen et al., 1995).

In order for a dendritic input to trigger a spike at the soma, the difference between V_{th} in the dendrite (which can be substantial; recall Fig. 19.3) and V_{th} in the axon needs to exceed the voltage attenuation between these two sites. This will allow dendritic input to trigger an axonal spike while remaining subthreshold within the dendritic tree, as demonstrated in Fig. 19.4. Panel A illustrates that the spike is initiated in the axon, subsequently propagating back through the soma into the apical dendrite at a speed of 150 μm/msec. In agreement with the data, the back-propagating spike is attenuated by a factor of 2 in amplitude as well as becoming broader in time. The former is due to the low density of sodium channels while the latter is caused by the distributed dendritic capacitance. Blocking the dendritic sodium channels does reveal, however, their boosting action on the back-propagating signal (Fig. 19.4C).

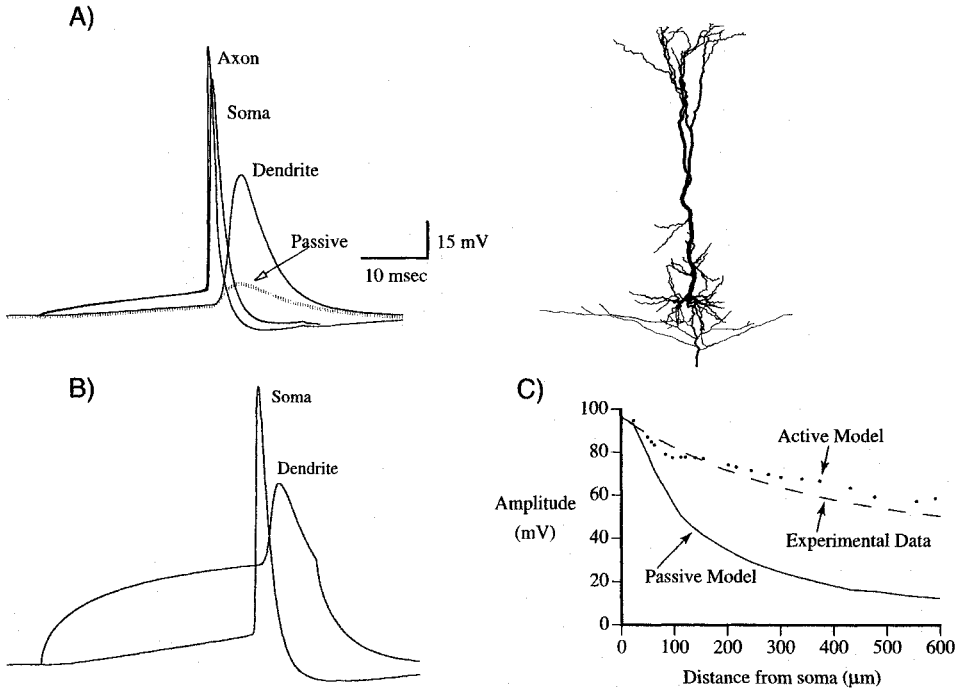

Fig. 19.4 SIMULATING ANTIDROMIC SPIKE INVASION Compartmental model of a layer 5 pyramidal cell from rat somatosensory cortex (shown at right; the vertical extent from the soma to the dendrite at the top is 1 mm) by Rapp, Yarom, and Segev (1996) with weakly excitable dendrites and cell body but a highly excitable axon. **(A)** Application of a 150-pA, 40-msec current pulse to the soma triggers an action potential at the axon (axon trace recorded 50 μm away from the soma). Within 0.5 msec it reaches the cell body and is propagating back into the dendrites (recorded 550 μm from the soma). Blocking the sodium current along the apical dendrite (dashed trace labeled "Passive") reveals the active nature of the back-propagating response. **(B)** Delivering a 300-pA, 40-msec current pulse to the apical dendrite causes a spike to be triggered at the axon and not locally, in the dendrite. This is due to (1) the passive load imposed by the dendritic arbor, (2) the lowered spiking threshold in the axon (m_∞ is shifted by 10 mV to more negative values compared to the dendritic sodium activation curve), and (3) the high sodium channel density at the axon ($\overline{G}_{Na}$ = 140 mS/cm^2). **(C)** Peak amplitude of the spike propagating back along the apical dendrite as a function of the distance from the soma. The dashed line corresponds to the experimental data of Stuart and Sakmann (1994) and is superimposed onto the output of the model (dots). When dendritic sodium channels are blocked ("Passive Model"), the active nature of the back-propagating response is revealed. $\overline{G}_{Na}$ ranges from 8 mS/cm^2 in the soma to 4 mS/cm^2 in the distal dendrites. Reprinted by permission from Rapp, Yarom, and Segev (1996).

The passive electrical load imposed by the dendrites and cell body, in combination with a weakly excitable dendritic tree and highly excitable axon, explains why spikes are always triggered in the axon and propagate back into the tree. How much the spike propagates back into the tree is controlled by a number of factors, such as the presence of transient potassium currents in the dendrites (Hoffman et al., 1997), inactivation of the sodium current by previous spikes (Migliore, 1996), and synaptic inhibition (Buzsaki et al., 1996; Tsubokawa and Ross, 1996).

Before we proceed further, it needs to be pointed out that most of the data upon which the modeling discussed in this section was based was obtained from pyramidal cells in relatively young rat slices. Developmental changes in channel densities and distribution (Huguenard,

Hamill, and Prince, 1988), local "hot spots" of sodium or calcium channels, the presence of neuromodulators, and other factors could well allow synaptic input to locally trigger action potentials in the dendritic tree.

19.3 Synaptic Input into Active Dendrites: Functional Considerations

From a computational point of view, passive dendrites can only instantiate a few elementary operations: (1) low-pass filtering, (2) saturation, and (3) multiplicative-like interactions among synaptic inputs. A much richer repertoire of nonlinear and nonstationary operations is possible if voltage-dependent membrane conductances are present in the dendritic tree.

In the remainder of this chapter, we discuss a number of specific operations that have been postulated to occur in excitable dendrites. The first one very briefly deals with the possible functional role of back-propagating spikes. The next two exploit precise coincidence detection using rapid and locally generated action potentials in spines and dendrites. The last two, involving graded amplification of distal synaptic input and multiplication with active conductances, consider dendritic all-or-none events as epiphenomena, focusing instead on the underlying voltage-dependent currents.

19.3.1 Back-Propagating Spike as Acknowledgment Signal

The role of back-propagating action potentials is puzzling if considered within the context of information processing, but makes more sense as an "acknowledgment signal" for synaptic plasticity and learning. We reviewed in Sec. 13.5.2 evidence by Markram et al., (1997) and earlier studies in favor of this hypothesis. By controlling the spike generation times in a pair of excitatory coupled neurons, the amplitude and time course of synaptic coupling between the neurons can be up or down regulated. If the presynaptic spike precedes the postsynaptic one, as should occur if the presynaptic one participates in triggering a spike in the postsynaptic cell, long-term potentiation occurs, that is, the synaptic weight increases. If the temporal order of arrival times is reversed (e.g., from +10 to -10 msec), long-term depression results. This provides the biophysical substrate for a novel class of powerful dynamic Hebbian synaptic learning rules for learning associations over time (e.g., Montague et al., 1995; Abbott and Blum, 1996; Gerstner et al., 1996).

19.3.2 Implementing Logic Computations with Spikes in Spines

In the chapter on dendritic spines (Sec. 12.4) we treated the idea of "spiking spines," that is dendritic spines that are endowed with a sufficient density of either sodium or calcium channels to be able to trigger all-or-none electrical events in the spine in response to a fast synaptic input (Segev and Rall, 1988). As summarized in Fig. 12.11, there exists a range of spine neck resistance values R_n, for which the induced EPSP in the passive dendrite just below the spine V_d is greatly amplified over the EPSP that would have been obtained if the spine had been passive. If R_n is too small, the high load of the dendritic tree increases V_{th} beyond the point at which synaptic input can trigger a spike. If R_n is too high, a spike is triggered but is highly attenuated by the time it reaches the dendrite.

Section 12.6.2 dealt with the experimental evidence using fluorescent dyes for all-or-none calcium events in individual spines (reviewed in Denk et al., 1996). Given the great difficulty in recording the membrane potential in spines and very thin dendrites, it

will be very demanding to verify directly the existence of fast sodium-mediated spikes in dendritic spines.

In Chap. 12 we restricted ourselves to treating single spines. More interesting from the point of view of neuronal computation are the combinatorial possibilities for nonlinear interactions among multiple active spines. As demonstrated by compartmental modeling (Shepherd et al., 1985; Shepherd and Brayton, 1987; Rall and Segev, 1987; Shepherd, Woolf, and Carnevale, 1989; see also Baer and Rinzel, 1991), one or a small number of simultaneous inputs to active spines can trigger action potentials in neighboring spines, providing a rich substrate for computations.

Zador, Claiborne, and Brown (1992) and Fromherz and Gaede (1993) have explored similar ideas relating to the implementation of the exclusive OR (XOR) operation using voltage-dependent currents in dendrites rather than in spines.

Active spines can interact with each other as long as the dendritic membrane potential V_d in response to synaptic input to some active spines is sufficient to trigger an action potential in those spines that did not receive any input. Recall that the voltage attenuation from the dendrite into the spine is basically nonexisting (Fig. 12.13). Thus V_d only needs to be large enough to exceed V_{th} in the spine (which decreases monotonically as R_n increases; Segev and Rall, 1988). A large value of V_d can be more easily obtained in the distal dendritic tree with its associated high input impedance.

Given the very high density of spines (up to 10 spines per micrometer; Sec. 12.1.1), what type of interactions might occur on distal dendrites? Rall and Segev (1987) explore this issue on the basis of an idealized neuron modeled by an equivalent cable with a trunk and five levels of symmetrical branches. The two most distal levels of dendrites are each endowed with 45 passive and 5 active spines. The parameters are chosen in such a way that a fast ($t_{\text{peak}} = 0.2$ msec) AMPA input to the spine triggers a local action potential, giving rise to a dendritic EPSP of 8.5 mV and a somatic EPSP of 24 μV (Fig. 19.5A; the somatic EPSP for an identical input to a passive spine is half of this amplitude). The local V_d is not sufficient to bring the other four active spines on this branch to threshold. However, two simultaneous inputs to two active spines will do the job, firing off the other three active spines that did not receive synaptic input (Fig. 19.5B). With an appropriately set threshold, this branch implements a logic OR, such that any two inputs to active spines will generate the same amplified output response (the peak somatic response in B is about 84 μV).

Triggering all five active spines simultaneously depolarizes the neighboring sibling branch sufficiently to trigger all of its active spines (Fig. 19.5C). It typically takes a millisecond or less for the spines that did not receive any direct synaptic input to trigger action potentials. In Fig. 19.5D, any two inputs to active spines on one branch and input to any three passive spines are sufficient to trigger all active spines on the two distal spines. Because the firing is more synchronous than in Fig. 19.5C, it sets off—with a delay—the active spines in the parent branch. Finally, Fig. 19.5E illustrates what could occur with inhibition targeting specific active spines, preventing a local action potential from being generated.

In principle, very specific higher order logical interactions could be implemented by active spine clusters. In practice, though, it is unclear whether the brain possesses specific enough developmental and learning rules that would guide an axon to form a synapse on one specific spine on one specific branch. The demanding requirements of which spine needs to be activated at what point in time in order to obtain a specific interaction renders them possibly not robust enough to be implemented in the nervous system. Further below we will deal with a much more robust mechanism, which exploits voltage-dependent inward

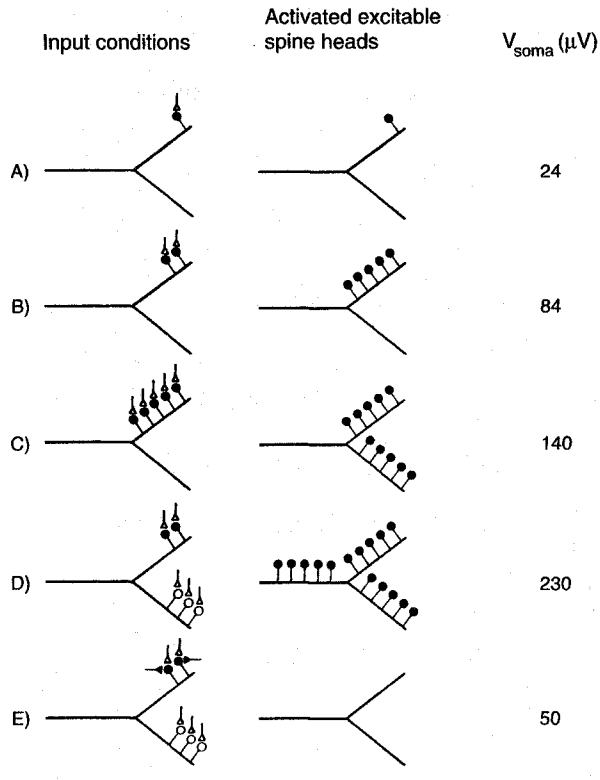

Fig. 19.5 Interacting Active Spines in the Distal Dendritic Tree Clusters of highly excitable dendritic spines can implement very specific interactions. Rall and Segev (1987) simulate an idealized dendritic tree with five levels of symmetrical branching, of which only the last two are shown. Each of the three branches carries five spines that include sufficient sodium and potassium channels to give rise to a rapid action potential and 45 passive spines. **(A)** Rapid synaptic input to a single active spine is sufficient to trigger a local action potential (see Fig. 12.10) that depolarizes the soma by 24 μV, while input to a passive spine would only depolarize the soma by 12 μV. **(B)** Two simultaneous inputs to two active spines raise the dendritic membrane potential sufficiently to trigger spikes in the remaining three active spines in this branch, but not in its sibling. **(C)** This can be accomplished by exciting all five active spines. **(D)** Two synaptic inputs to active spines on one branch and three to passive spines on the other will give rise to a wave of depolarization that is synchronous enough (compared to **C**) to trigger the active spines in its parent branch. **(E)** If fast inhibition is paired with fast excitation, no spikes are triggered, demonstrating the potentially large number of very specific interactions that can be implemented with active groups of spines. The open question is whether this mechanism is robust enough to be implemented within the central nervous system. The excitable membrane uses standard Hodgkin–Huxley-type Na^+ and K^+ conductances at five times their densities and adjusted for 20 C°. Reprinted by permission from Rall and Segev (1987).

currents—but not dendritic spiking—to implement a form of multiplication in spirit related to the computations presented here.

19.3.3 Coincidence Detection with Dendritic Spikes

One of the guiding themes of Chap. 15 has been the question to what extent individual nerve cells can be treated as "integrators," adding up many small synaptic inputs over tens of milliseconds, or as "coincidence detectors," firing in response to the exact temporal

relationship at the millisecond scale (see, in particular, Sec. 15.3.2). This issue is intimately connected to how much information (in terms of bits per spike or the reconstruction error; Gabbiani and Koch, 1998) single neurons can convey about a stimulus in the world. For stimuli varying on a time scale of a few milliseconds, submillisecond resolution at the single cell level should be superior in terms of efficiency of information encoding compared to representing the same information in the firing rate of a population of units that integrate over 20, 50, or more msec (Knight, 1972a; Softky, 1995). Of course, high-fidelity neurons place substantial demands on developmental mechanisms to arrange for the required precise interneuronal wiring. The advantage of a simple code carried by a population of integrator unit lies in their robustness to noise and in their simpler self-assembly requirements.

As investigated already by Segev and Rall (1988; see the preceding section), dendritic spikes provide a convenient biophysical mechanism for high-fidelity coincidence detection (Softky and Koch, 1993; Softky, 1994). We here discuss a recent model of a pyramidal cell discriminating spikes with a resolution in the 0.5 msec range (see also Sec. 5.2.3).

Softky (1995) endows the layer 5 pyramidal cell's dendrites with weakly excitable Hodgkin–Huxley conductances that are barely sufficient to sustain local regenerative events in the basal dendrites. This amounts to choosing $\overline{G}_{Na}$ to be 6 mS/cm^2, a twentyfold reduction of the maximal conductance in the squid axon and about one standard deviation above the mean value of 4 mS/cm^2 reported in rat neonatal apical dendrites (Stuart and Sakmann, 1994). Potassium conductances (with $\overline{G}_K = 1.8$ mS/cm^2) and time constants are chosen such that a single excitatory AMPA synaptic input (with $t_{peak} = 0.24$ msec) to the center of each thin terminal basal dendritic branch (Fig. 19.6A) yields a subthreshold response, while two simultaneous inputs are sufficient to trigger a very rapid all-or-none dendritic event of 40 mV or more amplitude. This signal is attenuated fiftyfold at the soma (Fig. 19.6B). If the same two EPSPs are separated by a mere 2 msec, the peak somatic EPSP is three times smaller. That the local potential in the basal dendrites can be exquisitely sensitive to the arrival times of synaptic input was already evident in the small value of the local delay $D_{ii} = 1$ msec (Fig. 3.13), which is much less than $\tau_m = 20$ msec.

This small time window for significant interaction among synaptic input is put to use by Softky by adding a third, inhibitory synaptic input (of the $GABA_A$ type with $t_{peak} = 0.4$ msec) to the same basal branch. Conjoint activation of all three inputs more or less nulls out the membrane potential, while a mere 1 msec delay between the simultaneous onset of the pair of excitatory inputs and inhibition fails to prevent the dendritic spike (Fig. 19.6C).

Softky (1995) simulates a triplet of synaptic inputs, with both fast excitatory inputs arriving simultaneously, followed 1 msec later by fast inhibition, placed at the midpoint of each of the terminals of the basal tree. Each triplet occurs independently of the others and is activated at a rate of 25 Hz. The result is that the pyramidal cell fires vigorously at about 55 Hz (Fig. 19.7A). What happens if the arrival times of all three elements is jittered in time (using a Gaussian distribution of standard deviation σ and assuming that on average the two excitatory inputs coincided and are followed 1 msec later by inhibition)? One such trial run with $\sigma = 0.5$ msec jitter is illustrated in Fig. 19.7B. The cell's firing is greatly reduced since dendritic spikes are absent. Figure 19.7C reports the average firing rate of the cell to repeated trials for a range of values of σ. The cell's response drops steeply with increasing σ, with a half-width at half-height of about 0.27 msec.

There is little indication in the somatic voltage record (Fig. 19.7A and B) of the very strong and transient dendritic signals that give rise to this temporal sensitivity.

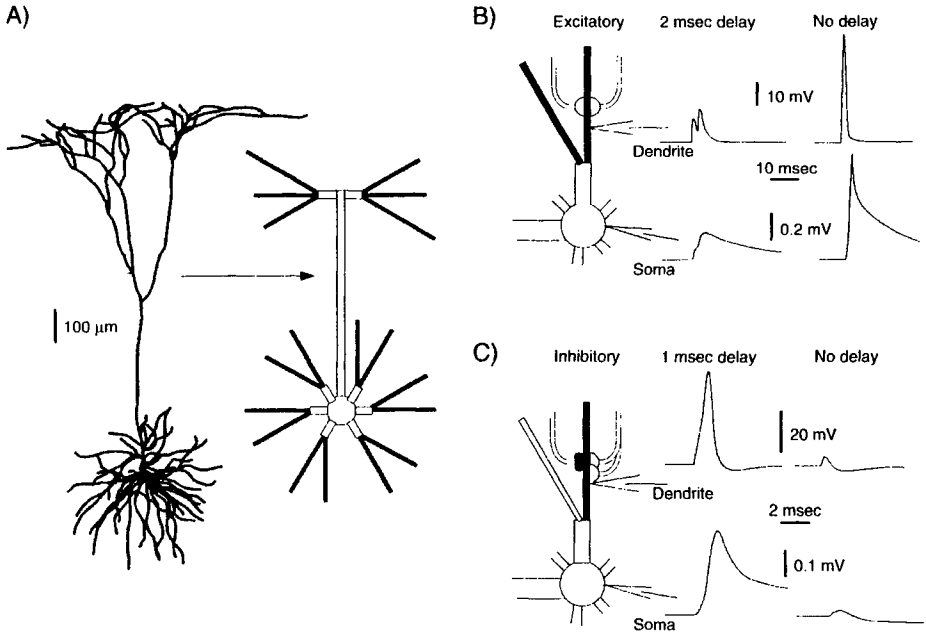

Fig. 19.6 Coincidence Detection with Dendritic Spikes Dendritic spikes initiated in response to local synaptic input can implement submillisecond temporal discrimination (Softky, 1994, 1995; see also Segev and Rall, 1988). **(A)** The standard layer 5 pyramidal cell is outfitted with weakly excitable dendrites and a strongly excitable cell body. Two fast excitatory synapses and one fast inhibitory synapse are placed along the center of each distal basal dendritic compartment. **(B)** The conductances are adjusted such that activation of a fast excitatory input to a basal dendrite, followed 2 msec later by a second such input, gives rise to a small local EPSP, while simultaneous activation of both triggers a very rapid all-or-none event, three times stronger than if the same synaptic events were separated by 2 msec. **(C)** If inhibition follows the two excitatory inputs by a mere 1 msec, it has little effect on the peak EPSP. Yet when all three synaptic elements are activated simultaneously, V_m remains close to rest. The voltage-dependent membrane conductances are of the Hodgkin–Huxley type with $\overline{G}_{Na} = 6$ mS/cm^2 in the dendrites. Reprinted by permission from Softky (1995).

The reason we discuss this study is that it demonstrates how, on the basis of a biophysically plausible parameter range, temporal coincidence detection with submillisecond resolution might occur. This mechanism could be exploited by the nervous system to implement a temporal code in which the exact (to within 0.5 msec or less) time of spiking relative to other neurons carries all of the relevant information (Softky, 1994). Such a temporal encoding strategy appears to be used in the insect olfactory system (Laurent, 1996; Wehr and Laurent, 1996). Given the combinatorial possibilities for expressing messages by shifting spike times around, it is considerably more powerful than a firing rate code that averages spiking from a population of cells over 50 msec or more.

As pointed out above, this does place a premium on the nervous system having learned how to compensate for axonal propagation and other delays in the system. The study by Markram et al., (1997) provides hope for the existence of such a mechanism at the level of an individual synapse, opening the door to learning rules that explicitly deal with delays.

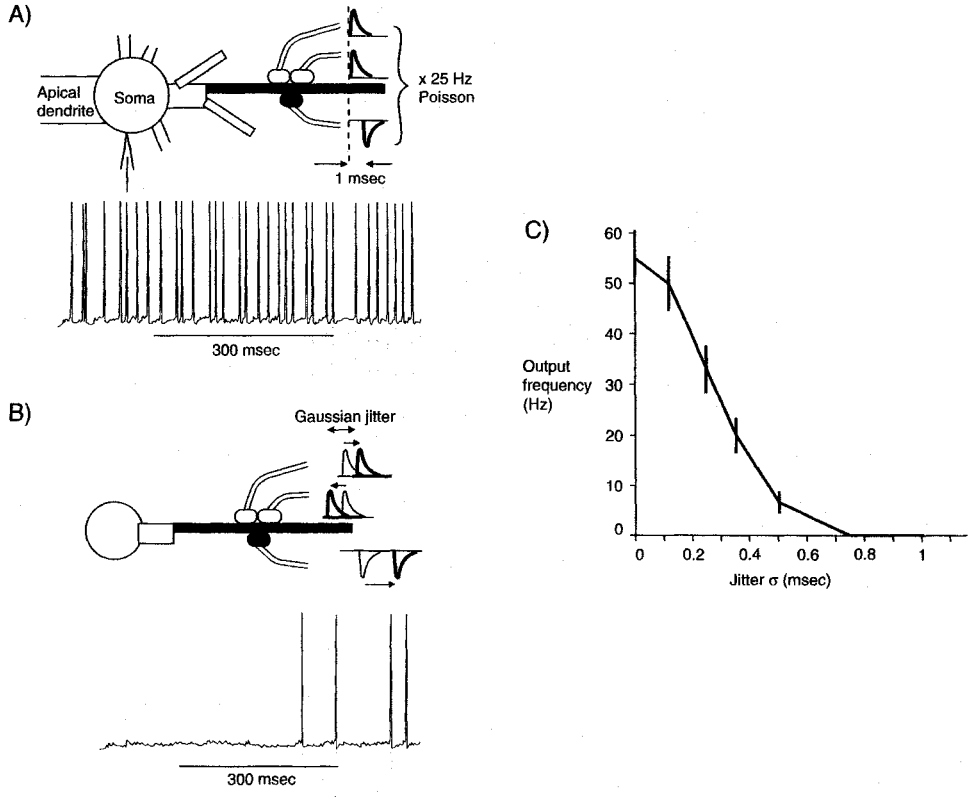

Fig. 19.7 SUBMILLISECOND COINCIDENCE DETECTION The model of Softky (1995) responds sensitively to jitter in the arrival times of synaptic input. This mechanism could be exploited to encode information in the relative spiking times of a group of neurons. **(A)** If all basal dendrites are endowed with weak Hodgkin–Huxley conductances and with the three synaptic elements illustrated in Fig. 19.6 that are activated independently of each other at 25 Hz, the somatic EPSPs due to the dendritic spikes summate, causing the cell to fire vigorously at 55 Hz. Note that one "synaptic event" here implies two simultaneously activated excitatory inputs followed 1 msec later by inhibition. **(B)** Adding jitter to the activation times of all synapses (the jitter is drawn from a Gaussian distribution centered at zero and with a standard deviation of σ) eliminates dendritic spikes, causing the cell to fire only weakly (illustrated here for $\sigma = 0.5$ msec). **(C)** Output firing rate as a function of σ; an average jitter of 0.27 msec in all three synaptic activation times causes the output to drop twofold. Reprinted by permission from Softky (1995).

19.3.4 Nonlinear Spatial Synaptic Interactions Using Active Currents

While the previous section dealt with temporal interaction among synaptic inputs in an active dendritic tree, let us now turn toward spatial interactions.

Chapter 5 treated nonlinear interaction among synaptic inputs. Due to the dependency of the NMDA membrane conductance on the postsynaptic membrane potential (Eq. 4.6), the EPSP in response to the simultaneous (or near-simultaneous) activation of two or more NMDA synapses can be much larger than the sum of the EPSPs due to the activation of each input by itself. The closer these synapses are spaced to each other, the larger the EPSP (Fig. 19.8B). Cooperativity among NMDA synapses needs to be contrasted to

the suppressive interactions among neighboring voltage-independent synapses in a passive dendritic tree. Due to the reduction in the driving potential and the absence of any mitigating increases in the synaptic-induced conductance change, the resultant EPSP will always be less than the sum of the individual synapses (Fig. 19.8A). Mel (1992, 1993) shows how this sensitivity to synaptic placement can be exploited to implement a robust multiplicative operation in the dendritic tree.

How does the addition of voltage-dependent dendritic calcium and sodium conductances impact the neuron's sensitivity to spatial clustering of synapses? Mel (1993) investigates this problem by randomly distributing a total of 100 synapses in clusters of k synapses each over the dendritic tree, where k ranges from 1 to 15 (see also Sec. 5.2.1). Each synapse is activated independently by a 100 Hz Poisson point process using one of several different postsynaptic scenarios. In one, all synaptic input is of the AMPA type, which is voltage independent, but the dendritic tree of the layer 5 pyramidal cell (Fig. 5.6) is endowed with

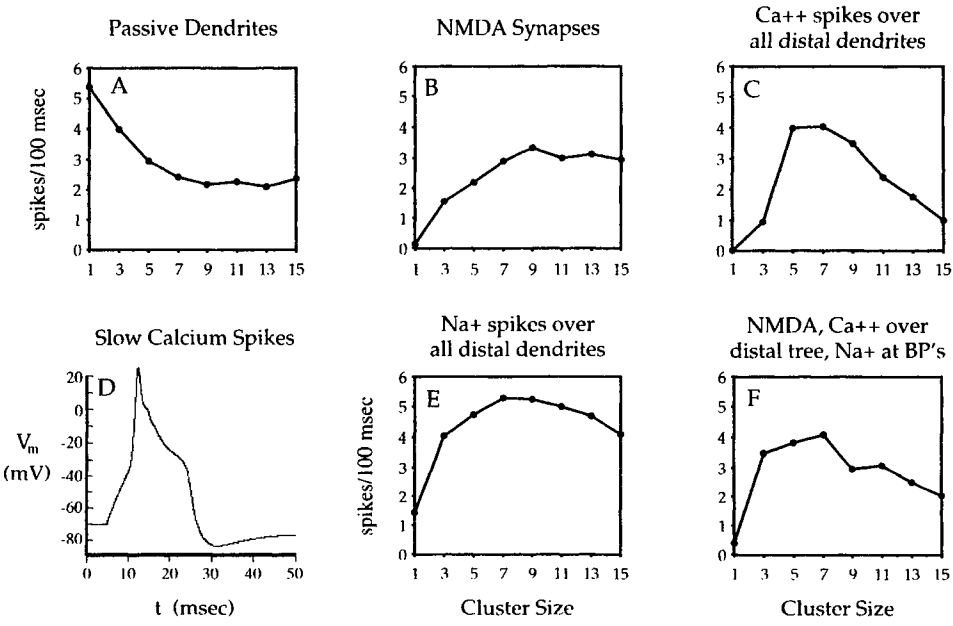

Fig. 19.8 Spatial Clustering of Synapses in an Active Dendritic Arbor Effect of spatial proximity of synaptic input on the cellular response in the presence of voltage-dependent dendritic membrane conductances. Mel (1993) distributes 100 synapses in 100/k clusters of k synapses each throughout the layer 5 pyramidal cell (Fig. 5.6) and activates each of them independently with a 100-Hz presynaptic train of spikes. The cellular response, expressed as the number of somatic action potentials within 100 msec, is averaged over 100 different random synaptic distributions. **(A)** For a passive dendritic tree and voltage-independent synaptic input, synaptic saturation dictates that spreading the synapses as far away from each other will maximize the cell's response. **(B)** Shifting 90% of the synaptic conductance to NMDA receptors favors activating spatially adjacent synapses. **(C)** In the presence of g_{Ca} and g_{AHP} in the distal portion of the tree, a similar cluster sensitivity results (here for AMPA input only). **(D)** This synaptic input frequently triggers a slow all-or-none dendritic event as portrayed here. **(E)** Replacing the slow dendritic g_{Ca} with fast Hodgkin–Huxley-like sodium spikes makes little difference as does the scenario summarized in **(F)**, a combination of calcium conductances in the distal dendritic tree with sodium spikes at dendritic branch points in the presence of strong synaptic input of the NMDA type. Reprinted in modified form by permission from Mel (1993).

a L-type high-threshold, noninactivating calcium conductance g_{Ca} in conjunction with a calcium- and voltage-dependent potassium conductance g_{AHP} (as well as radial diffusion and calcium buffering). These conductances are evenly distributed throughout the tree with the exception of the most proximal 60 μm stretch of each basal dendrite and the first 450 μm long section of the apical shaft, which are devoid of any such conductances. Under these circumstances, a sufficiently strong synaptic input can trigger a slow all-or-none dendritic event (Fig. 19.8D).

This gives rise to a very pronounced cluster sensitivity (Fig. 19.8C). Arranging the synaptic input into 20 clusters of five synapses each quadruples the cell's spiking response at the soma compared to clustering the same synapses in 33 groups of three synapses each. Replacing the dendritic g_{Ca} by a rapidly activating sodium conductance in conjunction with a delayed-rectifier potassium conductance yields fast dendritic spikes that lead to an inverted U-form cluster dependency (Fig. 19.8E). Finally, a last block of trials consists of the slow and distal calcium-conductance scenario, coupled with fast Hodgkin–Huxley membrane conductances at all dendritic branch points (distal 40 μm segment of each distal apical branch and the distal 40 μm of each apical and basal dendritic tip) and NMDA synaptic input (Fig. 19.8F). These and many more permutations of parameters (different conductances with different voltage dependencies, different patterns of synaptic input, and so on) always yield the same robust sensitivity of the cell's response to the spatial patterning of synaptic input.

Mel, Ruderman, and Archie (1998) demonstrate in a convincing manner how this nonlinear synaptic interaction can implement a crucial operation found throughout sensory systems. The best characterized neurons in the mammalian visual cortex are *simple cells*, whose distinguishing feature is that they respond optimally to visual stimuli (such as a bar) having a particular orientation (e.g., horizontal) at some position within their narrow receptive field (Hubel and Wiesel, 1962). A *complex cell* differs in a number of ways from a simple cell, chiefly in that it shows orientation tuning at many locations throughout its receptive field, which is much larger than the optimal bar stimulus. The transition from simple to complex cells is common to many systems and occurs anytime some selectivity, be it for disparity, face detection, and so on, must be generalized across space.

The original Hubel and Wiesel (1962) model as well as subsequent models (Movshon, Thompson, and Tolhurst, 1978; Heeger, 1992) posit that this tuning across space is accomplished by pooling the output of a set of simple cells with different receptive field positions. However, much evidence has accumulated challenging the notion of a purely hierarchical processing. In particular, complex cells receive direct, monosynaptic input from the lateral geniculate nucleus (LeVay and Gilbert, 1976; Ferster and Lindstrom, 1983; see also Malpeli et al., 1981; Ghose, Freeman, and Ohzawa, 1994). Mel and colleagues (1998) show how the center-surround receptive field of geniculate cells can be transformed in a single step into oriented complex cells using intradendritic computations.

The principal idea is similar to Mel's (1993) study of pattern discrimination using synaptic clustering (Sec. 5.2.2 and Fig. 5.9). As before, the layer 5 pyramidal cell receives mixed AMPA/NMDA excitatory synaptic input from a number of geniculate cells (either 100 or 1000). The dendritic membrane of the cell incorporates the standard g_{Na} and g_K Hodgkin–Huxley conductances, whose density is one quarter of the somatic density, in qualitative agreement with Stuart and Sakmann's (1994) findings discussed above. Mel, Ruderman, and Archie (1998) mimic a developmental learning rule that preferentially encourages the growth of geniculo-cortical synapses into the neighborhood of those patches of dendritic membrane that already show strong depolarization (Shatz, 1990; Cline, 1991).

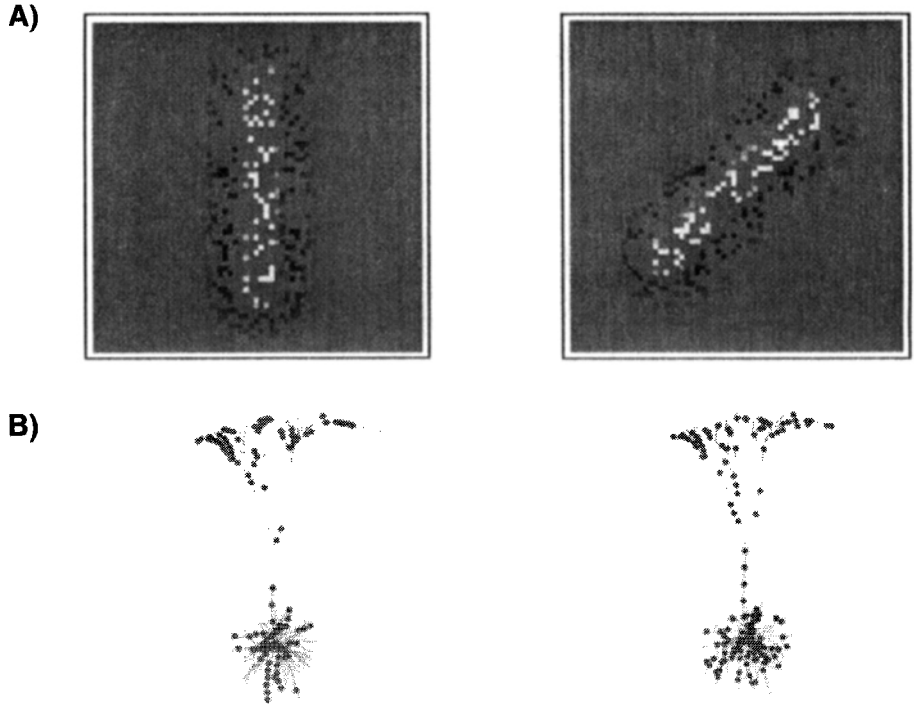

Fig. 19.9 Orientation Tuning in a Complex Cell in Visual Cortex The sensitivity of the firing rate to the exact spatial arrangement of synapses in the dendritic tree is exploited by Mel, Ruderman, and Archie (1998) to implement nonlinear superposition. This is exemplified by replicating orientation selectivity at multiple locations in the receptive field of a complex cell in the primary visual cortex directly excited by neurons in the lateral geniculate nucleus. The dendritic tree of the pyramidal cell includes sodium- and potassium-dependent Hodgkin–Huxley conductances. **(A)** Input is provided by 1024 randomly sampled geniculate cells that activate mixed—NMDA and AMPA—synapses (white squares; the black squares indicate inhibited cells). **(B)** A developmental rule for mapping these inputs onto the cortical cell assures that geniculate input activated by a vertical bar anywhere in the receptive field is organized in spatial clusters along the dendrites, while the synapses activated by an obliquely oriented input activate an equal number of synapses that are spread homogeneously throughout the dendritic tree (the 150 most active synapses are shown here).

This local activity could be caused, for instance, by simultaneous active synapses on a neighboring patch of dendrite. An outcome of learning rules of this type is that strongly correlated inputs are more likely to form synapses at nearby sites in the dendritic tree. In the case of Fig. 19.9, geniculate input is correlated with respect to an ensemble of vertically oriented bars form neighboring synapses (within less than 100 μm of each other along the dendrite) while geniculate inputs triggered by diagonally oriented bars are spread throughout the dendritic tree. This results in the formation of clusters corresponding to a set of geniculate afferents aligned in such a way as to be maximally activated by a vertical bar and least by a horizontal one.

With many such clusters, the cell shows orientation selectivity throughout its receptive field (Fig. 19.9D). The bar stimulus will always activate roughly the same number of synapses; but for nonoptimal orientations these are spread diffusely throughout the cell and their postsynaptic response is reduced. That orientation tuning is mediated by cluster

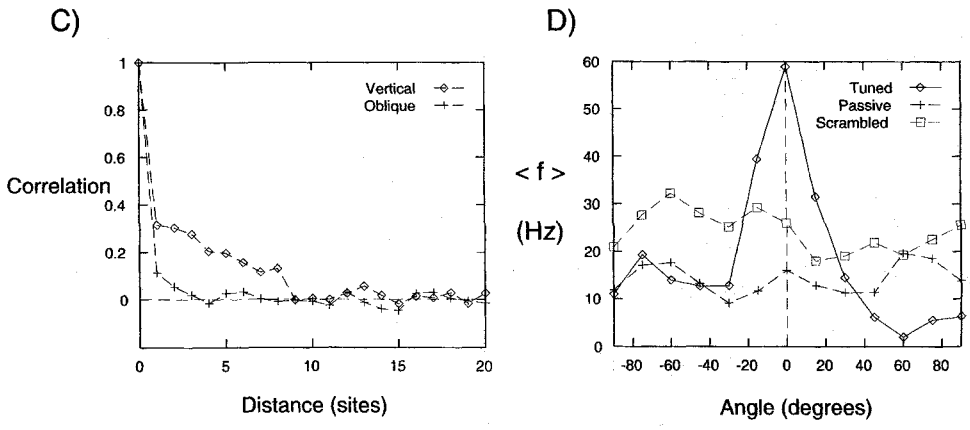

Fig. 19.9 CONTINUED (C) The spatial correlation function for synaptic input as a function of distance along the dendrite bears this out: for a vertical bar, synaptic input to the tree is correlated in space (up to approximately 100 μm). This spatial clustering leads to an optimal activation of NMDA and voltage-dependent inward currents. Very little such correlation is evident for the oblique input. (**D**) Averaging the spiking response of the cell for bars of different orientations presented at six different spatial positions yields a tuning curve very similar to those recorded in the cat visual cortex (Orban, 1984). Spatially scrambling the synapses or blocking the NMDA input and the dendritic g_{Na} (in this latter passive scenario, the AMPA conductances were amplified thirtyfold to compensate for the loss of current) eliminates orientation tuning. Reprinted in modified form by permission from Mel, Ruderman, and Archie (1998).

sensitivity caused by voltage-dependent conductances can be demonstrated in two ways: scrambling the spatial location of all synapses (that is, the mapping from the geniculate to the cortical cell is randomized) or blocking both the NMDA and dendritic g_{Na} conductances, which eliminates orientation selectivity (Fig. 19.9D). Mel, Ruderman, and Archie (1998) conclude that the position independence of orientation tuning of complex cells in the primary visual cortex could originate within the dendritic tree of a single cell, rather than by the convergence of the output of many cortical simple cells as usually assumed. Functionally, such a neuron corresponds to a polynomial threshold unit, computationally more powerful than the standard linear threshold unit (Sec. 14.4.2).

Note that this sort of nonlinear superposition might well be commonplace. Take as an example neurons in the most anterior portion of the inferotemporal cortex that strongly fire to a unique view of a three-dimensional object, such as a paperclip or a face, almost anywhere within the monkey's visual field (Logothetis and Pauls, 1995). They could achieve this feat by exploiting the same biophysical mechanism: nonlinear interaction among adjacent synapses in an active dendritic tree.

19.3.5 Graded Amplification of Distal Synaptic Input

In the previous chapter, we derived an analytical relationship between synaptic input to one end of a single finite cable and the current necessary to clamp the membrane potential at the other terminal (Eq. 18.18). As illustrated in Fig. 18.8, this current saturates once the synaptic input is large enough to depolarize the local membrane potential close to the synaptic reversal potential. This insight was extended to synaptic input into the distal apical tuft of the layer 5 pyramidal cell (Fig. 18.10C). The total somatic current that can be

delivered by 500 AMPA synapses distributed throughout layers 1, 2, and 3 (all the dendrites past the first major branch point along the apical tree; see Fig. 18.6) saturates at 0.65 nA, which is not enough to generate more than a handful of spikes per second at the soma. The culprit is the high axial resistance of the apical trunk, causing V_m in the distal dendrite to quickly approach the synaptic reversal potential. And this in a cell whose apical trunk is quite thick (4.4 μm diameter in the middle of layer 5; see Fig. 3.7) and has relatively low input impedances (see Table 3.1). The thinner dendrites in a rat pyramidal cell (Larkman and Mason, 1990) would give rise to even smaller values of $I_{\text{syn,s}}$.

It seems odd that a large fraction of the dendrite would be dedicated to synaptic input (in this case, originating to a large extent in higher cortical areas) that only has a minor effect on the output of the cell. Following earlier suggestions by Spencer and Kandel (1961) and more recent authors, Bernander, Douglas, and Koch (1994) investigated how voltage-dependent membrane conductances in the dendrites could be used to amplify distal synaptic input in a continuous manner.

Let us first consider the principle of the idea with the aid of a highly simplified model of a neuron (Fig. 19.10A). The three compartments crudely mimic the distal synaptic input (at right), the intervening apical tree (middle compartment), and the cell body, whose membrane potential is clamped to the average potential $\langle V_m \rangle$ during spiking (Fig. 17.10B). In the absence of any voltage-dependent membrane conductance, $I_{\text{syn,s}}$ will saturate (as in Eq. 18.18).

Because such saturation reduces the dynamic bandwidth of the input, Bernander, Douglas, and Koch (1994) argue that a voltage-dependent potassium conductance g_K needs to be introduced within the synaptic compartment in order to counteract saturation. The current does this by providing a hyperpolarizing current proportional to the degree of membrane depolarization. We can derive the voltage dependency of this current by demanding that

$$I_{\text{syn,s}} = \kappa_1 g_{\text{syn}} \,. \tag{19.1}$$

In the absence of g_K, $I_{\text{syn,s}}$ equals I_{syn}, the current flowing through the synapse (Fig. 19.10B). Kirchhoff's current conservation law demands that the current supplied by g_K must equal the difference between these two currents, that is, $I_K = I_{\text{syn,s}} - I_{\text{syn}}$.

From Fig. 19.10B this difference current has a parabolic shape: in the absence of synaptic input $g_K = 0$; likewise around $g_{\text{syn}} = 180$ nS, when the curves overlap again. At intermediate values of g_{syn}, activation of g_K makes up for the discrepancy between the two curves. Combining these equations, we find that the closed-form solution for the voltage dependency of g_K is a simple fractional polynomial (Fig. 19.10C),

$$g_K(V) = \frac{g}{2 \cdot \kappa_1} \frac{(V - V_{\text{soma}})(V - E_{\text{syn}} + \kappa_1)}{E_K - V} \,. \tag{19.2}$$

As the membrane potential depolarizes, g_K activates and opposes this increase. At large values of V, g_K inactivates, similar to the transient inactivating A type potassium current (Sec. 9.2.1), leading to an overall linear relationship between input and output, with $\kappa_1 =$ 5 mV (Fig. 19.10B). Amplification of this "linearized" current, that is,

$$I_{\text{syn,s}} = \kappa_1 \kappa_2 g_{\text{syn}} \tag{19.3}$$

can be achieved by an inward current between the synaptic site and the soma. Depending on the local membrane potential, it will generate additional current across the membrane. The derivation of the voltage dependency of the associated noninactivating conductance g_{Ca} is tedious but straightforward (done in Fig. 19.10C for $\kappa_2 = 2$). Note that different

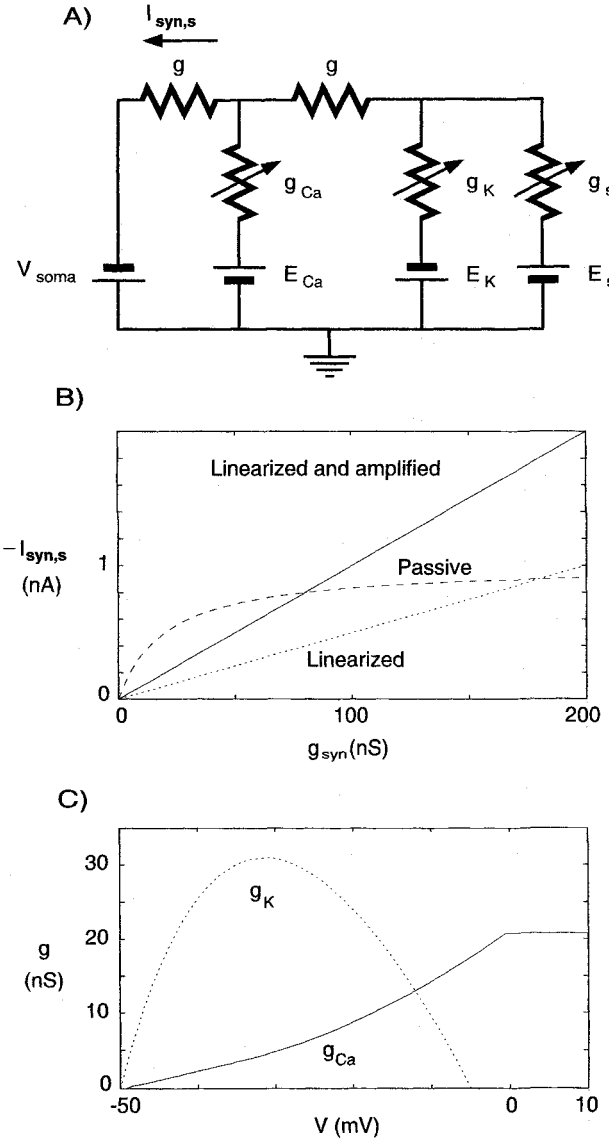

Fig. 19.10 PRINCIPLE OF DENDRITIC AMPLIFICATION Linearization and amplification in the three-compartment model shown in **(A)** with $V_{soma} = -50$ mV. All capacitances have been neglected. **(B)** "Somatic" current I_{soma} flowing across the conductance g in response to a sustained synaptic input g_{syn}. Due to synaptic saturation in the rightmost compartment, the current is sublinear (dashed "Passive" curve). The introduction of an inactivating potassium conductance g_K with the voltage dependency shown in **(C)** linearizes $I_{syn,s}$ as a function of g_{syn} (dotted "Linearized" curve). Positioning an inward current (here g_{Ca}) between the synaptic input site and the soma amplifies the synaptic response (thin "Linearized and amplified" curve). Reprinted by permission from Bernander, Douglas, and Koch (1994).

combinations of κ_1 and κ_2 in Eq. 19.3 give rise to different voltage dependencies for the potassium and calcium currents, but to the same current as long as the product $\kappa_1\kappa_2$ remains constant.

By analogy with this simple model, the saturating behavior of synaptic input into the apical tuft for the pyramidal cell of Fig. 3.7 can be eliminated by evenly spreading a noninactivating potassium conductance throughout layers 1, 2, and 3. The determination of its exact voltage dependency is carried out using an iterative learning scheme that modifies $g_K(V_m)$, recomputes $I_{syn,s}$, and changes its activation curve proportional to the difference between the actual somatic current and the desired linear one (Bernander, 1993). For reasons of stability, potassium inactivation was not considered here (unlike the simple model of Fig. 19.10C). Subsequently, an inward current is inserted into the membrane around the first branch point of the apical dendrite (close to the layer 3 to layer 4 transition) and

its activation curve is derived (Fig. 19.11B); it resembles a noninactivating high-threshold calcium conductance. Imaging experiments have visualized such a localized band of calcium activity 500 μm away from the cell body in neocortical pyramidal cells (Yuste, Delaney, and Tank, 1994).

In the presence of these two dendritic currents, distal synaptic input into the model cell delivers up to 1 nA of current to the soma (Fig. 19.11A), triggering 40 spikes per second in the absence of any other input (Fig. 19.11C). This sizable contribution is specific to apical tuft input (Bernander, Douglas, and Koch, 1994). Basal input will not be amplified since the calcium conductance is too far removed from the soma. The effect of the linearizing and amplifying currents remains hidden from the cell body and does not show up in the cell's f–I curve.

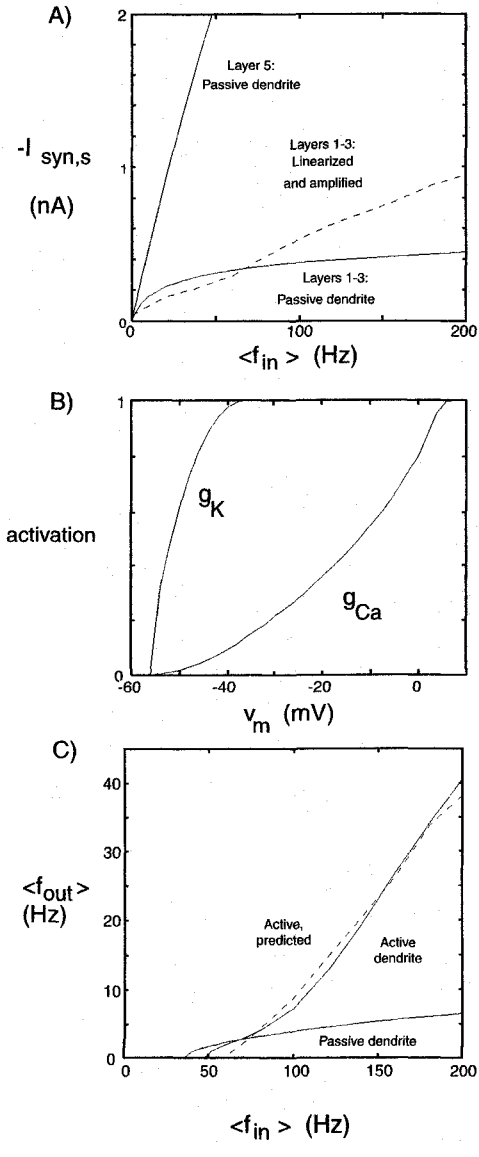

Fig. 19.11 Dendritic Amplification in a Pyramidal Cell The dynamic output range of the synaptic input into the apical tuft of the layer 5 pyramidal cell can be expanded via noninactivating voltage-dependent calcium and potassium conductances (Bernander, Douglas, and Koch, 1994). **(A)** The total somatic current delivered by 500 voltage-independent synaptic inputs into layers 1, 2, and 3 saturates quickly (see also Fig. 18.10). Spreading a potassium conductance g_K into all compartments in the apical tuft (beyond the major branching point of the apical dendrite in Figs. 3.7 and 18.6) and adding a hot spot of calcium conductances g_{Ca} at this branch point (with the voltage dependency shown in **B**) linearizes and amplifies the somatic current I_{soma} (dashed line in **A**). The final input-output relationship of the cell in **(C)** (computed by either clamping the soma to the mean somatic membrane potential or without restraining V_{soma} in any way) reveals that the distal input can modulate the cell's output firing rate in a significant manner. The function of these dendritic outward and inward currents is to linearize and amplify distal synaptic input. In this view, all-or-none calcium spikes are a mere epiphenomenon. Reprinted by permission from Bernander, Douglas, and Koch (1994).

The model treated here is quite simple and neglects many important aspects, such as calcium current inactivation, the detailed dynamics of the conductances, the effect of multiple calcium and potassium or other conductances, and so on. Furthermore, the exact distribution and voltage dependency of the two currents are only derived in a heuristic *ad hoc* manner. Yet the conclusion is similar to that of a biophysically more sophisticated simulation of active currents in cerebellar Purkinje cells (DeSchutter and Bower, 1994a,b): voltage-dependent inward dendritic currents can counteract the attenuation of distal synaptic inputs. In the Purkinje cell, this renders the somatic EPSP independent of the position of the synaptic input.

In this view, any all-or-none voltage events mediated by the amplifying inward current in the dendrites reflect a mere exuberance, an epiphenomenon. What is relevant is that the limited range of the current delivered to the soma is expanded by linearization and amplified in a graded manner.

A much more elegant and principled way of introducing a multitude of voltage-dependent dendritic currents is based on local, unsupervised learning rules that adjust the dynamics and the voltage dependency of the conductances. Such algorithms are related to the synaptic learning rules treated in Chap. 13 and achieve homeostasis by keeping the average calcium concentration at some setpoint (LeMasson, Marder, and Abbott, 1993) or by maximizing a quantity such as the mutual information between synaptic input and the output of the cell (Bell, 1992). Such learning schemes can operate continuously throughout the lifetime of the cell.

19.4 Recapitulation

It was held for a long time that voltage-dependent membrane conductances were restricted to the cell body and axon. Given the overwhelming evidence for the presence of a variety of sodium, calcium, and potassium conductances in the dendritic tree it is imperative that such active membranes be included into biophysically realistic compartmental models. We must also understand the functional role of such conductances.

Because of the great diversity of voltage-dependent currents found in so many different cell types throughout the animal kingdom, it is difficult to summarize the experimental data. The dendritic membrane of many neurons, in particular pyramidal cells, contains a relatively low but homogeneous distribution of ionic channels. This is enough to support the propagation of spikes from the axon and soma back into the dendritic arbor. That the spike is initiated in the axon and not locally in the dendrite can be explained by the fact that the difference in voltage threshold for spike initiation in the dendrite and V_{th} in the axon (due to much higher densities of active channels and/or intrinsic activation curves that are shifted toward more hyperpolarized values) is less than the voltage attenuation from the dendrite to the site of spike initiation

Under certain conditions, both rapid (1 msec) all-or-none sodium spikes and slower (10–50 msec) calcium-based action potentials can be observed in the dendritic tree. These may or may not propagate to the soma. The extent to which faster or slower spikes are initiated under physiological conditions in the dendrites and propagate to the soma remains unclear.

Numerous specific functions have been ascribed to active dendritic conductances, some dependent on dendritic spikes while others work in the absence of action potentials. Among the former resides the hypothesis that the timing of the back-propagated spike relative to the timing of any near-simultaneous presynaptic input is a crucial variable controlling whether

the weight of the associated synapse decreases or increases. A number of researchers simulated the ability of locally generated spikes in dendrites and spines to instantiate various logical operations as well as temporal coincidence detection.

Two quite plausible proposals for the functional role of active inward currents in the dendrites see them as providing the biophysical substrate either to implement a multiplicative-like operation in a distributed fashion among spatially clustered groups of synapses (the neuron as a sigma-pi element) or to linearize and amplify distal synaptic input selectively so that this input can modulate the cell's discharge more effectively (dendritic amplifier). Any such proposal raises many more questions than it answers, one of the most pertinent one being the question of the necessary developmental and learning rules that can assemble all of this hardware with the required temporal and spatial specificity (that is, inserting a certain number of channels of a specific type into a specific location at some subneuronal site). While a passive dendritic tree would require much less specificity to "wire up," its computational abilities are far less than those of an active dendritic arbor.